Current Biology 24, 1700–1711, August 4, 2014 ©2014 Elsevier Ltd All rights reserved http://dx.doi.org/10.1016/j.cub.2014.06.048

Article

Mechanical Role of Actin Dynamics in the Rheology of the Golgi Complex and in Golgi-Associated Trafficking Events

David Guet,[1,2,3] Kalpana Mandal,[1,2] Mathieu Pinot,[1] Jessica Hoffmann,[1,4] Yara Abidine,[1,5] Walter Sigaut,[1,6] Sabine Bardin,[1] Kristine Schauer,[1] Bruno Goud,[1,*] and Jean-Baptiste Manneville[1,*]
[1]CNRS-Institut Curie, UMR144, 26 rue d'Ulm, 75248 Paris Cedex 05, France

Summary

Background: In vitro studies have shown that physical parameters, such as membrane curvature, tension, and composition, influence the budding and fission of transport intermediates. Endocytosis in living cells also appears to be regulated by the mechanical load experienced by the plasma membrane. In contrast, how these parameters affect intracellular membrane trafficking in living cells is not known. To address this question, we investigate here the impact of a mechanical stress on the organization of the Golgi complex and on the formation of transport intermediates from the Golgi complex.
Results: Using confocal microscopy, we visualize the deformation of Rab6-positive Golgi membranes applied by an internalized microsphere trapped in optical tweezers and simultaneously measure the corresponding forces. Our results show that the force necessary to deform Golgi membranes drops when actin dynamics is altered and correlates with myosin II activity. We also show that the applied stress has a long-range effect on Golgi membranes, perturbs the dynamics of Golgi-associated actin, and induces a sharp decrease in the formation of Rab6-positive vesicles from the Golgi complex as well as tubulation of Golgi membranes.
Conclusions: We suggest that acto-myosin contractility strongly contributes to the local rigidity of the Golgi complex and regulates the mechanics of the Golgi complex to control intracellular membrane trafficking.

Introduction

The Golgi complex plays a central role in intracellular membrane trafficking. Despite constant inbound and outbound membrane fluxes, the Golgi complex maintains a stable structure and a typical *cis*, *median*, and *trans* cisternae organization. The architecture of the Golgi complex is thought to result from interactions between Golgi membranes, the cytoskeleton, and a protein scaffold, the so-called Golgi matrix.

Although the microtubule cytoskeleton has been known to be involved in Golgi organization for a long time, new critical players in Golgi architecture have been identified in the past ten years (for a review, see [1]). The actin cytoskeleton in particular actively participates in the maintenance of the Golgi architecture [2]. Although technically difficult to visualize, actin and actin nucleators are associated with Golgi membranes [3–5], and perturbation of actin dynamics leads to disorganization of the Golgi cisternae [6, 7]. Myosins also localize to the Golgi complex [8] and have been involved in the formation of transport intermediates from the *trans* side of the Golgi complex [9–11], and myosin II-driven contractility is required for the fission of Rab6-positive vesicles [9]. Moreover, the formin mDia1, an activator of actin polymerization, has been recently implicated in the maintenance of the Golgi structure and the formation of Rab6-positive transport intermediates [12].

Experiments based on biophysical approaches have shown that mechanical parameters, such as membrane rigidity or tension, are critical for intracellular transport [13, 14]. Studies in living cells have focused on the plasma membrane [15]. Recently, mechanical stretching or osmotic swelling in cells and in vitro reconstitution on model membranes confirmed that a high mechanical load on the plasma membrane limits membrane invagination in both clathrin-dependent [16] and clathrin-independent [17] endocytosis. Similar data on intracellular compartments are lacking, mostly because accessing intracellular membranes for mechanical experiments in living cells is technically challenging.

In order to probe the architecture of the Golgi complex and test for the potential effects of a mechanical stress exerted on the Golgi complex on membrane trafficking, we designed a new intracellular micromanipulation technique based on the optical trapping of internalized micrometer-sized latex beads coupled with fast confocal imaging. The technique allows, for the first time to our knowledge, the application and measurement of a force up to a few hundreds of piconewtons on a fluorescently labeled intracellular organelle and simultaneously visualization of the induced deformation.

Results

Mechanical Deformation of Golgi Membranes

To apply and measure a force on Golgi membranes, we have developed an intracellular micromanipulation technique based on optical trapping of micrometer-sized beads. Latex beads (diameter 2 μm) were endocytosed overnight in RPE1 cells and accumulated in the perinuclear region (Figure 1A, top). The endocytic membranes surrounding the beads were tightly apposed on the bead surface and were negative for the early endosome marker Rab5 but positive for the late endosomal/lysosomal markers LAMP1 (Figure 1B) and CD63 (data not shown). A mechanical force was applied on the Golgi complex by pushing it against a bead held in a fixed optical trap (Figure 1A, bottom). The pushing force was generated by displacing the microscope stage. The force was measured by tracking the position of the bead (see Experimental Procedures) and the Golgi complex was simultaneously imaged by fast confocal microscopy. Using this technique, we were able to

[2]Co-first author
[3]Present address: Unité Pathologie et Virologie Moléculaire INSERM U944 CNRS UMR9212, Institut Universitaire d'Hématologie, Hôpital Saint-Louis, 1 avenue Vellefaux, 75010 Paris, France
[4]Present address: Ecole Normale Supérieure, 45 rue D'Ulm, 75230 Paris Cedex 05, France
[5]Present address: CNRS-Université Joseph Fournier Grenoble, Laboratoire Interdisciplinaire de Physique (LiPhy), 140 Avenue de la Physique BP87, 38402 Saint Martin d'Hères, France
[6]Present address: LMGP-Grenoble INP-Minatec, 3 parvis Louis Néel CS 50257, 38016 Grenoble Cedex 1, France
*Correspondence: bruno.goud@curie.fr (B.G.), jean-baptiste.manneville@curie.fr (J.-B.M.)

efficiently deform the Golgi complex by applying forces in the 100–200 pN range.

Golgi Membranes Are Flexible and Mechanically Coupled

The Golgi complex was visualized using GFP-Rab6 that localizes to *trans*-Golgi and TGN (*trans*-Golgi network) membranes and to small vesicles that shuttle between the Golgi complex and the cell periphery [9]. Rab6-positive Golgi ribbons were bent upon application of a mechanical force (Figure 1C, Movie S1 available online), showing that the Golgi complex is a flexible structure that can be deformed by ~100–200 pN forces. Similar results were obtained using another Golgi marker, GFP-tagged COPI subunit εCOP (data not shown). To investigate the effect of the applied force on the Golgi structure, we acquired projections of 3D confocal stacks before and after applying a mechanical constraint. In a control experiment, as expected, the two images could be superimposed (Figure 1D, No constraint). This was not the case after application of the force (Figure 1D, With constraint), indicating that structural changes are induced on Rab6-positive Golgi membranes by the mechanical constraint, both near and far (up to 10 μm) from the trapped bead (Figures 1D and 1E). These findings suggest that Rab6-positive Golgi membranes are mechanically coupled and that a rigid component propagates the constraint along Golgi membranes.

The Microenvironment Rigidity Increases Close to the Golgi Complex

To characterize the mechanical properties of the microenvironment of the beads when they approach the Golgi complex, we compared the local stiffness a few micrometers away from Rab6-positive Golgi stacks (Movie S2, left) with the stiffness measured in close proximity to Rab6-positive membranes (Movie S2, right). The cell was moved automatically via a two-axis nanopositioning piezo-stage in a stepwise fashion to bring Rab6-positive membranes initially about 1 μm away from the bead either into contact with the bead or alternatively farther away from the bead. Five 0.5 μm steps were performed during 1 min (Figure 2A) and the bead displacement was measured. The bead displacement depends on the viscoelastic properties of the surrounding microenvironment. Figure 2A depicts four expected behaviors.

We first tested the technique in cell extracts prepared either from *Xenopus* oocytes or from HeLa cells (Figure 2B, gray curves). In both cases the total bead displacement did not exceed 0.25 μm. In cells, after each 0.5 μm step displacement of the stage, the bead experienced a step increase followed by an exponential relaxation of its position toward the trap center. When the load on the bead became too high, the bead was ejected out of the trap (see Movie S2, right). The softness index, the bead step amplitude, and the relaxation time (parameters defined in Experimental Procedures) were calculated and compared between two conditions: Rab6-positive Golgi membranes were either moved away from the bead or moved toward the bead (Figures 2B and 2C). In the latter condition, the softness index decreased while the bead step amplitude and the relaxation time increased. In addition, the frequency of bead ejection from the optical trap was more than 5 times higher for beads brought close to the Golgi complex than for beads pushed away from the Golgi membranes toward the cytoplasm (Figure 2D).

By plotting the softness index measured when the beads were pushed toward the Golgi complex as a function of the distance separating the bead from the nearest Rab6-positive membrane, we could detect an increase in rigidity when the beads entered a region within 1.5 μm from the Rab6-positive Golgi membranes (Figure S1B). We confirmed this stiffening by measuring the complex shear modulus of the Golgi microenvironment using an oscillatory displacement of the piezo-stage (see Supplemental Experimental Procedures and Figure S1C). Both the storage modulus G' and the loss modulus G'' increased when regions closer than 1.5 μm to the Rab6-positive Golgi membranes were probed.

Taken together, these measurements indicate that the local microenvironment stiffens as the bead approaches the Golgi complex.

Actin Dynamics and Acto-Myosin Contractility Control the Rigidity of the Golgi Complex

We next investigated the role of actin and acto-myosin contractility in the mechanical properties of the Golgi complex.

In a first set of experiments performed on cells treated or not with cytochalasin D (cytoD), which induces actin depolymerization by binding to F-actin and impairing its polymerization, Rab6-positive membranes were pushed manually against the bead. In control cells, the force rapidly reached a plateau of about 100 pN, preventing further displacement (Figure 3A, see also Movie S3, left). In contrast, in cytoD-treated cells, the force dropped after each displacement of the cell, allowing the bead to penetrate between Rab6-positive Golgi membranes on distances up to 10 μm (Figure 3B, see also Movie S3, right). The maximum displacement was about 2.5 times higher in cells treated with cytoD than in nontreated cells (Figure 3C). The softness index increased with the concentration of cytoD. These results show that depolymerizing actin softens Rab6-positive Golgi membranes.

To quantify the role of actin in the local mechanical properties of the Golgi area, the pushing force was then applied by moving the cell automatically in a stepwise fashion as described above. The softness index, the bead step amplitude, and the relaxation time were measured in the presence or absence of cytoD and jasplakinolide, which blocks actin dynamics in cells by disrupting actin filaments and inducing polymerization of monomeric actin into amorphous masses. The two drugs had very similar effects (Figure 4A) and induced an increase in the softness index, a decrease in the bead step amplitude, and no significant effect on the relaxation time (Figure 4C). The frequency of bead ejection out of the trap dropped (Figure 4D). In contrast, no effect of actin depolymerization was detected when the trapped beads were pushed away from the Rab6-positive Golgi membranes (Figure S2).

To directly visualize the dynamics of polymerized actin before and after the application of the force, we used cells stably expressing LifeAct-mCherry and labeled with the live Golgi marker BodipyFL ceramide (Movie S4). We scored the frequency of dynamic actin patches in one confocal section during a 1 min time-lapse acquisition (Figures 5A and 5B) and the total number of actin patches in 3D reconstructions of the Golgi area (Figures 5C and 5D). We observed a decrease in both the frequency and the total number of actin patches. Two pathways have been implicated in actin polymerization at the level of the Golgi complex: the Cdc42/N-WASP-Arp2/3 pathway [18] and, more recently, the RhoA-formin (mDia1) pathway [12]. As shown in Figures 5E and 5F, the number of cortactin patches, an activator of the Arp2/3 complex, decreased in cells fixed after application of the force as compared to control cells in which no force was applied. In

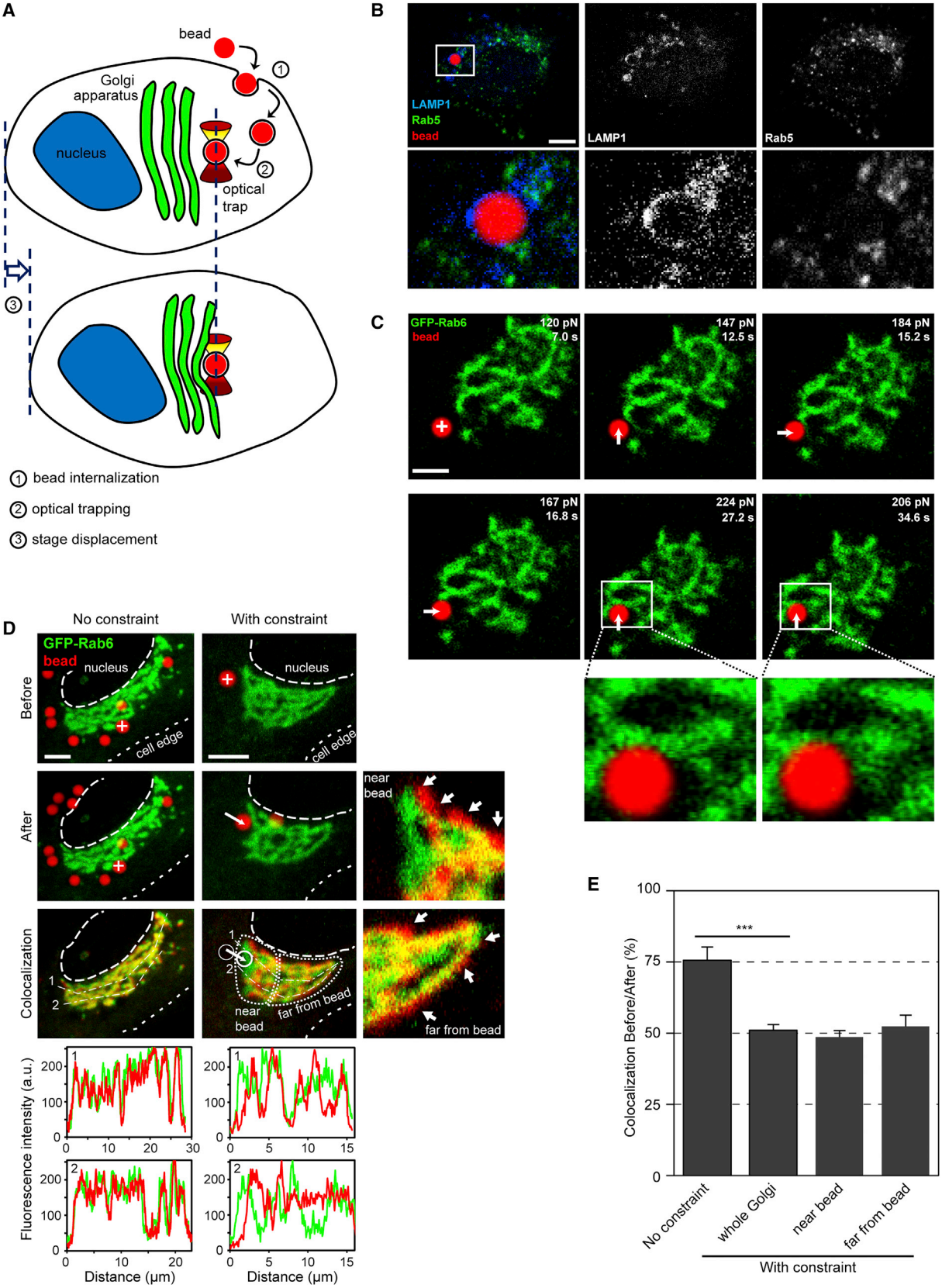

Figure 1. Probing the Mechanics of Golgi Membranes

(A) Experimental set up. 2 μm red fluorescent beads were endocytosed overnight in RPE-1 cells expressing GFP-Rab6 to visualize the Golgi complex (1). A bead located close to the Golgi complex was trapped using optical tweezers (2). Golgi membranes were then pushed against the bead held at a fixed

(legend continued on next page)

addition, the treatment of cells with SMIFH2, a formin inhibitor, led to effects very similar to those of cytoD or jasplakinolide, i.e., an increase in the softness index and a decrease in the bead step amplitude (Figures 4A, 4C, and 4D). This suggests that the two pathways regulating actin polymerization were affected by the mechanical constraint applied to the Golgi complex.

To test whether acto-myosin contractility could participate in the rigidity of the Golgi complex, we repeated the experiments described above in the presence of the myosin II activator calyculin A or the myosin II inhibitor cocktail ML7+Y27632 (Figure 4B). When myosin II was inhibited, the results were quantitatively similar to those obtained when actin dynamics was perturbed. The softness index significantly increased on average, whereas the bead step amplitude and the frequency of bead ejection decreased (Figures 4C and 4D). Opposite results were obtained when myosin II contractility was activated by calyculin A (Figures 4B–4D).

Taken together, the above results show that actin polymerization and acto-myosin contractility confers rigidity to the peri-Golgi region.

A Mechanical Stress on the Golgi Complex Induces Defects in Membrane Trafficking

We next investigated whether a mechanical force applied on the Golgi complex could affect the formation of Rab6-positive transport vesicles, a process that relies on the acto-myosin machinery [9]. Rab6 trafficking was imaged by confocal microscopy for 1 min. After trapping the selected bead, the cell was first moved during 1 min in order to bring the Rab6-positive Golgi membranes in closest proximity with the optically trapped bead. Visible deformation of these membranes was then obtained by applying a force in the 100–200 pN range while imaging Rab6 trafficking again for 1 min. In control experiments, the selected bead was trapped for 2 min without moving the stage. Recovery of membrane trafficking was assessed by capturing an additional 1 min movie of Rab6 trafficking 20 min after the constraint was stopped.

We observed a strong decrease in the number of Rab6-positive vesicles in the vicinity of the Golgi complex upon application of the force (Movie S5, corresponding to Figure 6A). To quantify the flux of Rab6 transport intermediates leaving from or arriving to the Golgi complex, we used a kymograph-based approach (Figure S3). A 2-fold decrease in the flux of Rab6 intermediates was measured after application of the mechanical force. This decrease was similar for the population of vesicles moving out of the Golgi region or the population of vesicles moving back to the Golgi complex. A partial recovery of Rab6 trafficking (80% of control) was observed after 20 min in the absence of force (Figure 6B). In addition, no significant alteration of the microtubule network in the vicinity of the Golgi was observed at the immunofluorescence level following bead displacement (Figures S4A and S4B).

In the majority of the cells (60%), the decrease in the number of Rab6-positive vesicles was accompanied by the formation of Rab6-positive tubules still connected to the Golgi (Movie S5 and Figure 6A). The average number of tubules increased more than 3-fold and their length doubled upon application of the force (Figure 6C). This phenotype is indicative of a fission defect as the KIF5B kinesin is pulling on Rab6-positive membranes that cannot detach from the Golgi [9]. A similar defect in fission was previously observed following inhibition of myosin II activity [9] or mDia1 depletion [12]. Altogether, these results suggest that applying a mechanical force on Golgi membranes impacts on actin dynamics and myosin activity, which are necessary for the production of Rab6-positive transport vesicles.

Contribution of Other Proteins to Golgi Rigidity

Although actin disassembly leads to a strong decrease in Golgi rigidity, the values of the mechanical parameters do not reach the levels measured away from the Golgi complex (Figure 2), suggesting that other elements participate in Golgi mechanics. Proteins of the Golgi matrix such as GRASPs or golgins [1] could also contribute to the Golgi rigidity. To test the role of the Golgi matrix, we depleted the Golgi matrix protein giantin using siRNA (Figures S5A and S5B) and repeated the viscoelastic relaxation experiments. We observed a 30% decrease in the rigidity of the peri-Golgi area when the expression level of giantin was reduced (Figures S5C–S5E), similar to the contribution of the actin cytoskeleton.

Discussion

A Novel Tool to Probe the Mechanics of Intracellular Membranes

Optical tweezers were used previously to trap and move a variety of intracellular organelles and to measure the forces exerted by molecular motors in vivo [19–22]. More recently, internalization of micrometer-sized beads followed by optical or magnetic trapping was used to measure motor forces

position in the optical trap by moving the microscope stage either manually via a joystick or automatically via a nanopositioning piezo-stage (3).
(B) The membrane surrounding the bead is positive for late endosomal and lysosomal markers. Left: RPE-1 cells were fixed and stained for Rab5 (green) and LAMP1 (blue) 5 hr after addition of the beads (red). A zoom of the boxed region is shown in lower images.
(C) Example of mechanical deformation of Golgi membranes visualized with GFP-Rab6 (green). Images shown are stills from a 1 min time-lapse movie (Movie S1). The position of the optical trap is indicated by a cross in the first image. The direction of the force is shown by an arrow and its magnitude is indicated in the top right corner of each image. The boxed areas in the last two images are shown on the lower images.
(D) Long-range effect of a mechanical constraint on Golgi membranes. Maximum projections of confocal stacks of a cell in which the Golgi membranes were pushed by manual displacement of the microscope stage against a bead held in the optical trap for 1 min (right column) and of a control cell in which no constraint was applied (i.e., the bead was trapped for 1 min without stage displacement, left column). The top and middle images show GFP-Rab6 in green and beads in red, respectively, before and after optical trapping. The bottom images shows the colocalization (yellow) of the GFP-Rab6 signals before (green) and after (red) optical trapping. Two higher-magnification images of regions near the bead and far from the bead are shown for the constrained Golgi complex. The position of the trap is indicated by a cross and the trapped bead is shown by circles in the colocalization images. Arrows in the high-magnification colocalization images point to zones where the shape of Golgi membranes is most affected by the mechanical constraint. Fluorescence intensity profiles along two dashed lines (1 and 2) are shown below the images (green, before application of the constraint; red, after application of the constraint).
(E) Graph showing colocalization of the GFP-Rab6 signals before and after optical trapping from the whole Rab6-positive Golgi area measured when no constraint was applied (n = 6 cells) and when a constraint was applied (n = 22 cells). In the case of a constrained Golgi complex, colocalization in a 5 μm-wide region close to the bead (near bead) and in the remaining Golgi area (far from bead) was measured. Both values are significantly decreased compared to control indicating both short- and long-range effects of the constraint. Error bars represent mean ± SEM.
Scale bars represent 5 μm. See also Movie S1.

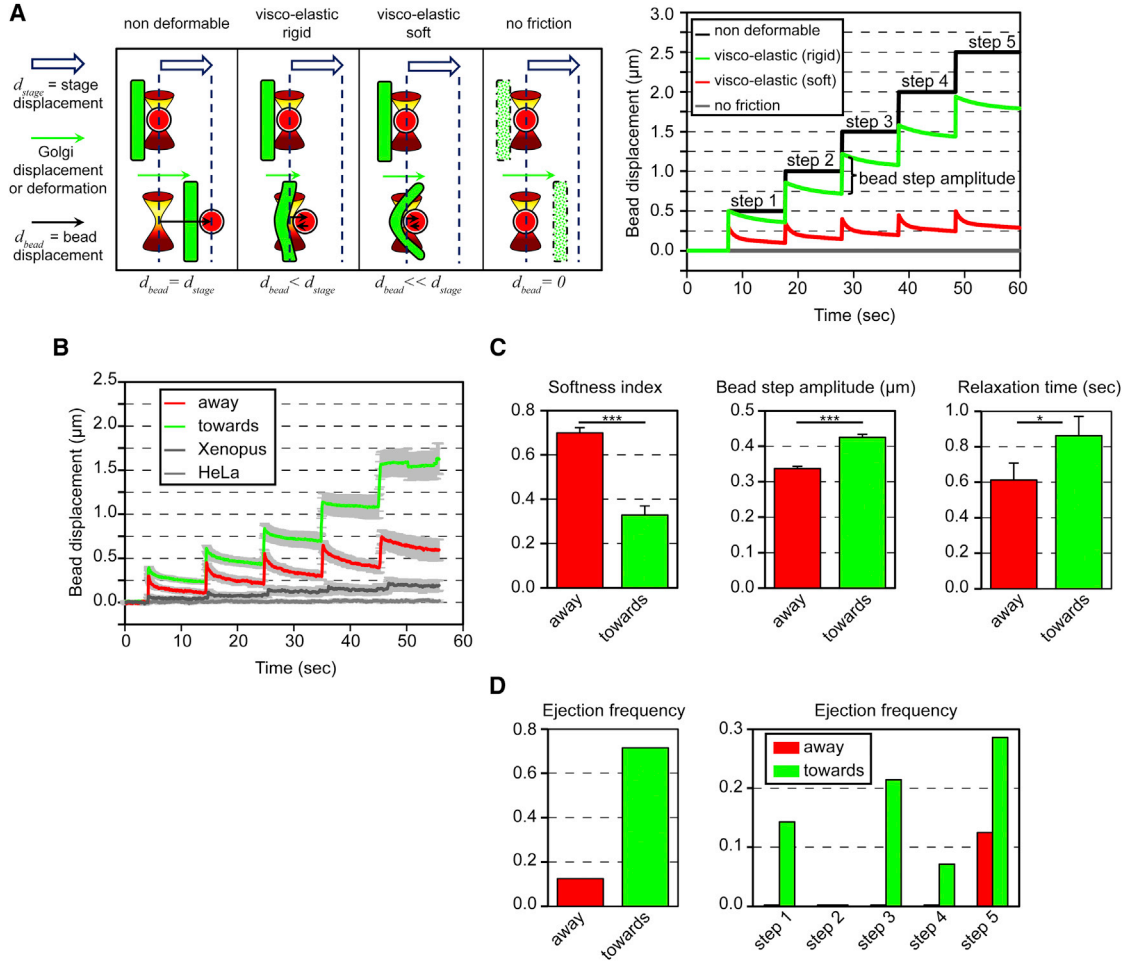

Figure 2. The Local Stiffness Increases in Proximity of the Golgi Complex

(A) Probing the visco-elastic properties of the bead microenvironment. Left: Schematics illustrating the position of the optical trap, the stage displacement (double blue arrow), the bead displacement (black arrow), and the displacement and/or deformation of the Golgi membranes (green arrow) in four model cases. From left to right: the Golgi complex is not deformable, the Golgi complex behaves as a rigid or soft visco-elastic material, and the Golgi complex exerts no friction on the bead. Right: Graphs showing the displacement of the bead after five 0.5 μm step displacements of the piezo-stage in the same four cases: (1) the bead is embedded in or contacts a very rigid nondeformable microenvironment (black line) and its position follows that of the stage ($d_{bead} = d_{stage}$); (2) and (3) the bead is embedded in a visco-elastic microenvironment and its position relaxes exponentially after each 0.5 μm step (green line for rigid; red line for soft); and (4) the bead is embedded in a microenvironment with vanishing viscosity that exerts a vanishing friction (gray line) and its position is not affected by the stage displacement ($d_{bead} = 0$).

(B) Rab6-positive membranes were pushed away from (red lines) or toward (green lines) a bead held in the optical trap by moving the piezo-stage using five 0.5 μm steps in 1 min (Movie S2). Grey curves show the same experiments performed in *Xenopus* oocyte extracts (dark gray) and HeLa cell extracts (light gray). The graph shows the averaged (n = 8 for "away," n = 25 for "toward," n = 16 for *Xenopus*, n = 11 for HeLa) displacements of the bead as a function of time. Error bars shown in gray represent mean ± SEM.

(C) Measurements of the softness index, the bead step amplitude, and the relaxation time in the cytoplasm ("away," n = 7 cells) or in close proximity of Rab6-positive membranes ("toward," n = 22 cells). Error bars represent mean ± SEM.

(D) Frequency of bead ejection from the optical trap in the cytoplasm ("away," n = 8 cells) or in the Golgi area ("toward," n = 14 cells) after five 0.5 μm steps (left) and frequency of bead ejection at each individual step (right).

See also Movie S2.

involved in endosome or phagosome transport [23–27]. We show here that optical trapping of an internalized bead can be used as a wedge to deform an intracellular organelle and measure the corresponding applied force. Using simultaneous fast confocal imaging, we are able to correlate the observed deformation with the measured force.

Two characteristics of our assay should be discussed. First, since they penetrate by phagocytosis, beads are surrounded by a membrane of late endosomal/lysosomal origin (Figure 1B). This membrane appears to be tightly apposed on the bead surface so that it should not perturb significantly the force measurements performed on the bead. The membrane could, however, mediate interactions with the cytoskeleton via molecular motors. Forces exerted by molecular motors and binding forces between motors and their cytoskeletal tracks are of the order of a few pN (see [28] and [29] for reviews and [24, 26, 27]). This suggests that the forces involved in our experiments (100–200 pN) induce detachment of the beads from the cytoskeleton. Accordingly, the diffusion of the bead was enhanced after displacing the bead by 0.5 μm, corresponding to a 100 pN force, from their initial position (Figure S1A).

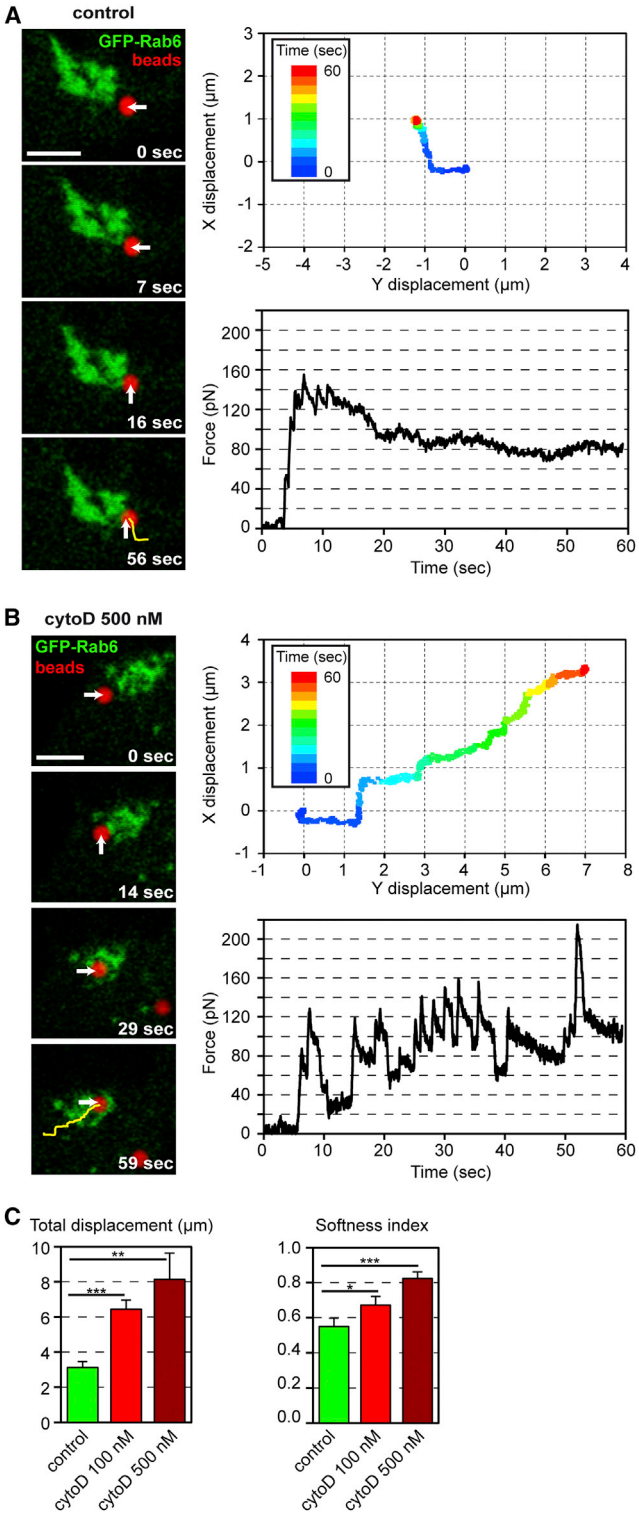

Figure 3. The Actin Cytoskeleton Contributes to the Rigidity of the Golgi Complex

(A and B) Actin disassembly facilitates bead displacement in the Golgi area and within Golgi stacks. Cells were treated (B) or not (A) with cytochalasin D at the indicated concentrations for 15 min. The Rab6-positive membranes (green) were manually pushed against a bead trapped in the optical tweezers (red, indicated by an arrow) for 1 min using a joystick controlling the microscope stage displacement (see Experimental Procedures for details). Typical relative displacements of the bead within the cell and corresponding force curves are shown in (C), right panels. The pictures on the left are stills from Movie S3 taken at the indicated time points. The total bead displacement is shown by a yellow line in the last picture.

(C) Measurements of the total relative displacement of the bead within the cell and of the softness index in control nontreated cells and in cells treated with 100 or 500 nM cytochalasin D (n = 22, 10, and 4 cells respectively). Error bars represent mean ± SEM.

Scale bars represent 5 μm. See also Movie S3.

A second issue concerns the size of the beads. The displacement of a 2 μm diameter bead within the cell could significantly alter intracellular organization, in particular the cytoskeleton. Forces required to break actin stress fibers, which contain not only actin but also myosins and actin crosslinkers, are of the order of 400 nN [30], three orders of magnitude larger than the forces applied by the bead. In our experiments, microtubule dynamics did not seem to be significantly altered by the displacement of the bead (Figures S4A and S4B). The timescale of our experiment (1 min) is similar to that of actin or microtubule dynamics [31, 32], suggesting that despite the large size of the bead, the displacement of the bead is slow enough to allow reorganization of the cytoskeleton. A weak impact of bead displacement on the microtubule cytoskeleton is further supported by the observation of Rab6-positive tubules that are pulled from Golgi membranes along microtubules [9] after application of the mechanical constraint (Figure 6). Finally, beads found in the perinuclear region did not contact the plasma membrane (Figure S4C), indicating that a potential effect of actin on force measurements should be solely due to actin bound to the Golgi complex and not to cortical actin. Depolymerizing actin had no effect on the force exerted on beads located a few micrometers away from the Golgi complex (Figure S2), further suggesting that our measurements are not sensitive to cortical actin.

Forces in the 100 pN Range Are Required to Deform the Golgi Complex

Visible deformation of GFP-Rab6 Golgi membranes was obtained upon application of 100–200 pN forces (Figure 1 and Movie S1), significantly higher than the forces required to deform lipid membranes, which are of the order of 10–50 pN. The viscous drag force due to the bead displacement within the cytosol, given by $F_{visc} = 6\pi\eta_{cyto}Rv$ (where η_{cyto} is the cytoplasm viscosity, R is the bead radius, and v is the velocity of the stage displacement), could contribute significantly to the total force exerted on the bead. Taking $R = 1$ μm, $v \approx 0.5$ μm/s, and $\eta_{cyto} \approx 10^2$–$10^4\eta_{water} \approx$ 0.1–10 Pa.s [33, 34], we find $F_{visc} \approx$ 1–100 pN depending on the value of the cytoplasm viscosity. However, because forces increase as the bead approaches the Golgi complex (Figures 2, S1B, and S1C), the viscous drag due the cytoplasm is clearly not the only player.

Microrheology of the Peri-Golgi Area

The microrheology assay we developed is particularly well adapted to probe the microenvironment of the Golgi complex. The measured parameters (softness index, bead step amplitude, relaxation time, and ejection frequency) are used here as global indicators of the Golgi mechanics independently of any visco-elastic model. To relate our measurements with standard rheological parameters, we developed a simple theoretical description based on a single Kelvin-Voigt element (a spring of elasticity E and a dashpot of viscosity η in parallel) to model the microenvironment of the bead (Supplemental Experimental Procedures and Figure S1D). As expected,

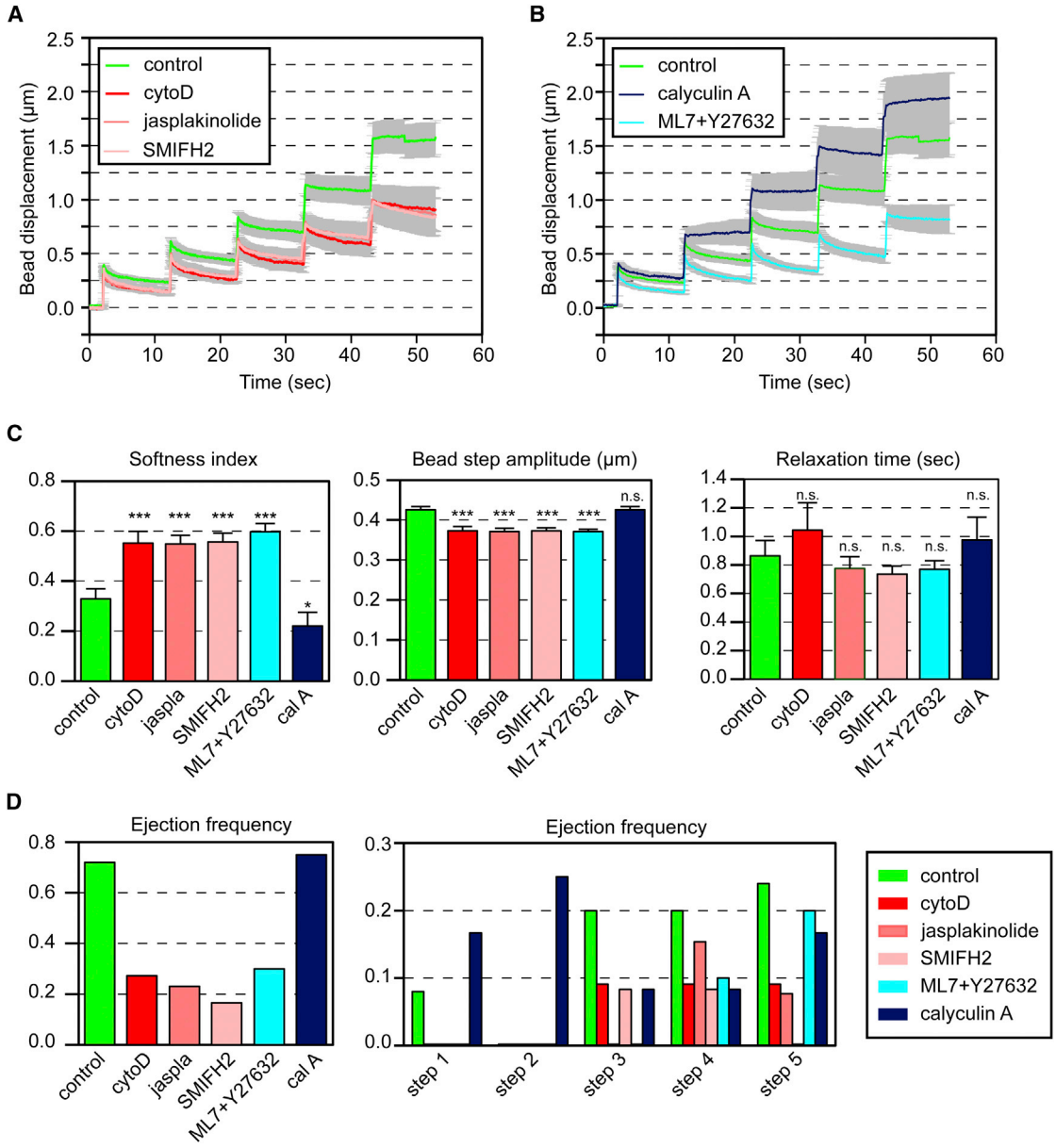

Figure 4. Influence of Actin Dynamics and Acto-Myosin Contractility on the Mechanics of the Golgi Complex

(A) Perturbing actin dynamics softens Golgi membranes. Cells were treated with 250 nM cytochalasin D (cytoD) for 15 min, 200 nM jasplakinolide (jaspla) for 30–60 min, or 25 μM SMIFH2 for 30–60 min. Rab6-positive membranes were then pushed toward a bead held in the optical trap by moving the piezo-stage using five 0.5 μm steps in 1 min as in Figure 2. The graph shows the averaged bead displacement in control cells (n = 25 cells) and in cells treated with cytochalasin D (n = 11 cells), jasplakinolide (n = 15 cells), or SMIFH2 (n = 12 cells) as a function of time. Error bars shown in gray represent mean ± SEM. Note that the curves corresponding to drug-treated cells are almost superimposed.

(B) Activating (resp. inhibiting) myosin II contractility stiffens (resp. softens) Golgi membranes. Cells were treated with the activator of myosin II contractility calyculin A (calA, 0.5 nM) for a maximum duration of 12 min or with the myosin II inhibitors ML7 (30 μM) and Y27632 (10 μM) for 20 min. The graph shows the averaged bead displacement in control cells (n = 25 cells) and in cells treated with calyculin A (n = 12 cells) or with ML7+Y27632 (n = 21 cells). Error bars shown in gray represent mean ± SEM.

(C) Softness index, bead step amplitude, and relaxation time in the same conditions as in (A) and (B) (n = 22, 11, 15, 12, 20, and 12 in control, cytochalasin D, jasplakinolide, SMIFH2, ML7+Y27632, and calyculin A conditions, respectively). Error bars represent mean ± SEM.

(D) Frequency of bead ejection from the optical trap after five 0.5 μm steps (left) and at each individual step (right) in the same conditions as in (A) and (B) (n = 22, 11, 15, 12, 20, and 12 in control, cytochalasin D, jasplakinolide, SMIFH2, ML7+Y27632, and calyculin A conditions, respectively).

See also Figure S2.

within this description, the softness index increases while the bead step amplitude decreases when both E and η decrease (Figure S1E). This simple model also accounts well for the short-term visco-elastic relaxation following a step displacement and the experimental data were fitted to obtain the elasticity E and viscosity η of the bead microenvironment (Figure S1G). These data show that both elasticity and viscosity more than double close to the Golgi complex.

Our measurements of the complex shear modulus of the Golgi microenvironment using an oscillatory displacement of

the stage further confirms our analysis in terms of softness index. When the distance to the Rab6-positive Golgi membranes decreases, a similar increase is observed for both the storage modulus G' and the loss modulus G'' (Figure S1C) as for the softness index (Figure S1B) or for the values of the elasticity and viscosity derived from the theoretical description.

Role of Actin and Acto-Myosin Contractility in the Mechanical Properties of the Golgi Complex

Previous electron microscopy studies showed that actin forms a cortex around Golgi membranes that could participate in tethering Golgi stacks [2]. We show here that the actin cytoskeleton plays a major role in the rigidity of the Golgi complex. The Golgi complex is stiffer than the surrounding cytoplasm (Figure 2) and this increase in stiffness is largely due to polymerized actin (Figures 3 and 4). In contrast, no effect of actin disassembly was measured in the cytoplasm (Figure S2) in agreement with a previous report [35]. The viscoelastic relaxation time τ was slightly but significantly larger in close proximity to the Golgi complex than in the cytoplasm (Figure 2C) with a value of $\sim$1 s, in the range of relaxation times of actin gels in vitro [36, 37] and of the cell actin cortex [38], further suggesting that the bead enters an F-actin layer when it is pushed on Golgi membranes. Interestingly, the mechanical constraint applied to the Golgi complex affected the two pathways that lead to actin polymerization (Cdc42/N-WASP-Arp2/3 and Rho-mDia1), suggesting that both contribute to actin dynamics at the Golgi.

Besides the structural role of actin, myosin II-dependent contraction appears to be crucial to maintain the rigidity of the Golgi complex and its high resistance to mechanical deformation (Figure 4). Another striking feature of the mechanical response of the Golgi complex is the acto-myosin-dependent ejection of the beads out of the optical trap (Figure 4D). Actin polymerization and acto-myosin contractility have been shown to be force dependent [39] on similar time scales as in our experiments, which could explain the response of the Golgi complex to load. Similar to the plasma membrane where the acto-myosin cortex is considered as an active gel that can exhibit shape instabilities [40], the Golgi structure could be actively regulated downstream of the mechanical constraint by an acto-myosin-dependent mechanism.

Mechanical Control of Membrane Transport

A mechanical constraint applied on the Golgi complex decreases the number of Rab6-positive vesicles and leads to the formation of Rab6-positive tubules connected to the Golgi complex. This phenotype is strikingly similar to that observed upon myosin II inhibition or mDia1 depletion on the dynamics of Rab6-positive intermediates [9, 12]. A likely interpretation of these results is that the mechanical constraint impacts actin organization, in particular via the Rho-mDia1 pathway, resulting in the inhibition of the fission of Rab6-positive vesicles and the appearance of tubular intermediates that cannot detach from Golgi membranes. Alternatively, the mechanical load on the actin cytoskeleton could modify the motor activity of myosin II [41]. Another possibility is that the mechanical constraint impacts membrane tension, since an increase in tension was shown in vitro to inhibit membrane deformation, which precedes the formation of transport vesicles [13, 17, 42]. In support of this hypothesis, we observed in a significant number of cells a decrease in the number of Rab6-positive vesicles without apparent tubulation of Golgi membranes.

Conclusion

We have developed a new technique to study the mechanics of intracellular compartments and obtained quantitative information on the architecture of the Golgi complex and on the dynamics of intracellular transport to and from this organelle. Our mechanical measurements showing a stiffening of the microenvironment in close proximity to Golgi membranes may have important implications for membrane targeting and fusion of vesicles with Golgi membranes and for intra-Golgi transport. Although actin appears to be crucial for Golgi mechanics, Golgi matrix proteins also probably play a role, as illustrated by the decrease in Golgi rigidity after giantin depletion. Future studies should aim at deciphering the relative contribution of the actin cytoskeleton, Golgi matrix proteins, and spectrins in Golgi mechanics.

Our results also suggest that a mechanical stress has a long-range impact on membrane trafficking by inhibiting membrane budding and/or membrane fission. It will be particularly interesting to follow the fate of a secreted cargo to determine whether secretion itself depends on the mechanical state of the Golgi complex. For instance, during development or during tumor formation, cells experience high compressive stresses that could be transmitted to intracellular organelles, in particular the Golgi complex, and thereby could impact membrane trafficking.

Experimental Procedures

Cell Culture, Cell Extracts, and Reagents

RPE-1 (human retinal pigment epithelial) cells were cultured in DMEM-F12 supplemented with 10% FCS. The stable cell line expressing GFP-Rab6 was described previously [43]. The stable cell line expressing εCOP-GFP was a gift from Cathy Jackson and Samuel Bouvet (Institut Jacques Monod, Paris, France). The stable cell lines expressing EB1-GFP and LifeAct-mCherry were gifts from Mathieu Piel (Institut Curie, Paris, France). For immunofluorescence experiments, cells were seeded on glass coverslips and fixed with 4% paraformaldehyde or methanol. Primary antibodies used were: anti-Rab5 (BD Biosciences #610724), anti-LAMP1 (BD Biosciences #555798), anti-βtubulin (Sigma #T4026), and anti-cortactin (Merck Millipore). Secondary antibodies were from Jackson ImmunoResearch Laboratories. The plasma membrane was labeled with CellMask Orange (exc 550 nm/em 570 nm) or CellMask Deep Red (exc 650 nm/em 670 nm) (Invitrogen). For live cell experiments, cells were seeded on glass-bottom dishes (MatTek Corporation, ref P50G-1.5-14-F) or glass-bottom dishes with a 50 μm mesh-size grid (Ibidi μ-dish) to relocate cells in which a mechanical constraint was applied after fixation. The live Golgi marker BodipyFL ceramide (Invitrogen) were used to label the Golgi complex in wild-type RPE-1 cells. In experiments where actin dyamics was perturbed, cells were treated with 100–500 nM cytochalasin D (Sigma) or 200 nM jasplakinolide (Merck Millipore) or 25 μM SMIFH2 (Merck Millipore). Myosin II activity was inhibited with a combination of the myosin light chain kinase inhibitor ML7 (30 μM, Sigma) and the Rho kinase inhibitor Y27632 (10 μM, Calbiochem) for 20–40 min [9]. Myosin II activity was increased with 0.5 nM calyculin A (Merck Millipore). Metaphase II-arrested *Xenopus* meiotic extracts were kind gifts from Zoher Gueroui (Ecole Normale Supérieure, Paris, France) and were prepared as described previously [44].

Intracellular Optical Micromanipulation

Our set-up is based on a previously described system combining optical trapping and confocal imaging (see Supplemental Experimental Procedures). Latex beads with diameter 2 μm (red fluorescent exc 580/em 605 ref F88265 from Invitrogen or Flash Red fluorescent exc 660/em 690 ref FS05F/9833 from Bangs Laboratories) were incubated overnight with the cells. Before the experiment, cells were washed once in PBS then imaged in culture medium supplemented with 20 mM HEPES. Typically 3–5 beads were internalized by cell and were found in the perinuclear area. Since the trapping force is proportional to the infrared laser intensity gradient and to the third power of the bead radius and because of the high viscosity of the cytoplasm ($\eta_{cyto} \sim 10^2$–$10^4 \eta_{water} \sim 0.1-10$ Pa.s [33, 34]), efficient trapping was possible only with large enough beads (2 μm in diameter) and at relatively

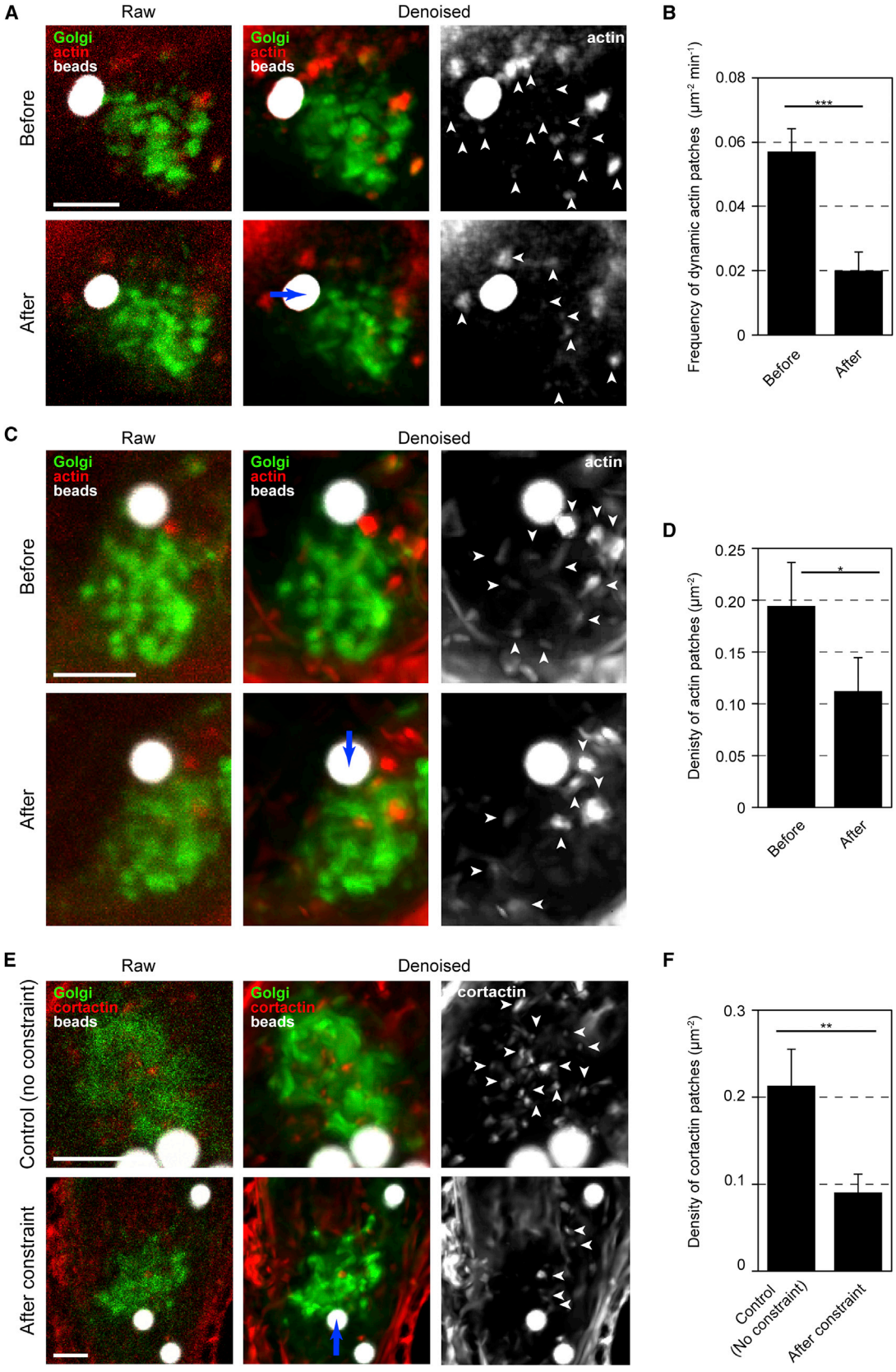

Figure 5. A Mechanical Constraint Induces Defects in Golgi-Associated Actin Dynamics

(A–D) A force was applied on the Golgi complex of LifeAct-mCherry-expressing cells by pressing Golgi membranes labeled with the live Golgi marker BodipyFL ceramide for 1 min against a bead held in an optical trap (see Movie S4).

(legend continued on next page)

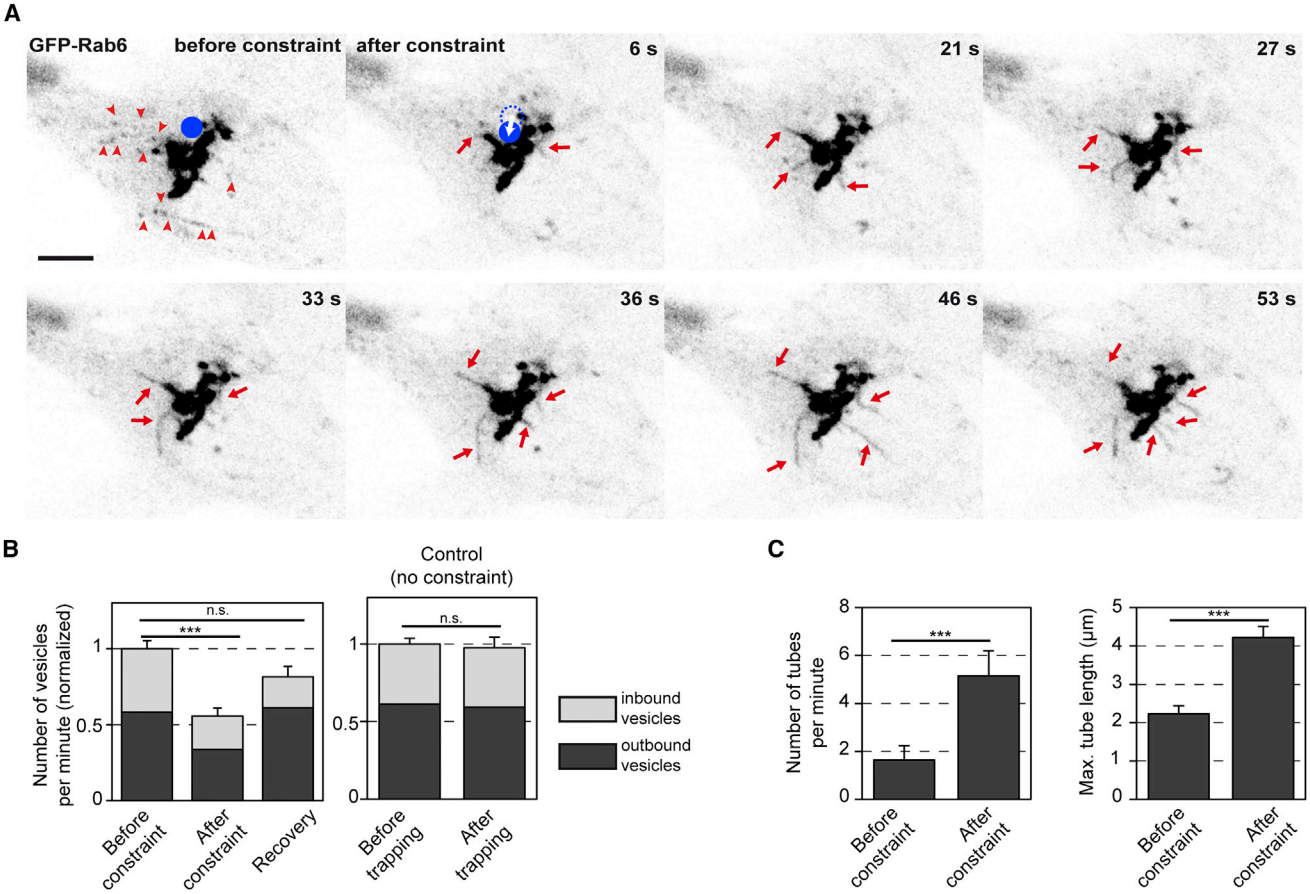

Figure 6. A Mechanical Constraint Induces Defects in Membrane Trafficking

(A) A force was applied on the Golgi complex by pressing Rab6-positive Golgi membranes for 1 min against a bead held in an optical trap (stills are from Movie S5). The position of the bead is indicated by a blue circle and the direction of the force by a white arrow. Vesicles are shown by red arrowheads before application of the constraint and tubes are shown by red arrows after application of a 1 min-long constraint. Scale bars represent 5 μm.

(B) Flux of vesicles entering (inbound) or exiting (outbound) the Golgi area before and after application of a 1 min-long constraint and after a 20 min-long recovery without force (n = 11 cells and 5 cells for recovery experiments). The number of vesicles is normalized by the value before optical trapping. In control experiments (right), the bead was trapped without applying a constraint on the Golgi complex as in Figure 1D (n = 12 cells). Error bars represent mean ± SEM.

(C) Frequency of Rab6-positive tubule formation and tube length before and after applying a force on the Golgi complex. Error bars represent mean ± SEM. See also Figures S3 and S4 and Movie S5.

high laser power (1W at the fiber output corresponding to ~145 mW after the objective). The total duration of optical trapping was limited to 2 min for a given cell. In these conditions, cell viability was not affected.

The force F acting on the optically trapped bead was measured by tracking the position of the bead x relative to the trap center x_0 according to $F = -k(x - x_0)$, where k is the trap stiffness. Calibration of our optical trap by the viscous drag method yielded a trap stiffness of k = 200 ± 10 pN μm^{-1} W^{-1}. Single-particle tracking of the bead imaged by confocal fluorescence microscopy at 15–30 frames/s was performed using a Matlab program (kindly provided by Gil Toombes and Patricia Bassereau).

To apply a force on the Golgi complex, a bead located close to Rab6-positive membranes was first trapped and the microscope stage was then moved to bring the Golgi complex in contact with the bead. Stage displacement was performed either manually using the microscope joystick in the "constant speed" mode set at the lowest possible value (0.5 μm/s) (see Supplemental Experimental Procedures) or automatically using the nanopositioning piezo-stage controlled by the NanoRoute3D software (Mad City Labs) for microrheological measurements as described below.

Microrheological Measurements and Analysis

Five 0.5 μm steps in x or y direction were performed by piezo-controlled stage displacement. Each step was followed by a 10 s pause (see Figure 2A). This protocol allowed pushing a bead on distances up to 2.5 μm into an intracellular compartment. After a 0.5 μm piezo-stage displacement step, the bead could either relax toward the center of the trap or, if the viscous drag was larger than the trapping force, fall off the optical trap. In the latter

(A and B) Time projections of a 1 min movie before (top) and after (bottom) the application of a mechanical constraint. The frequency of actin patches colocalizing with the Golgi marker was scored as the number of dynamic LifeAct-mCherry patches visible during the 1 min movie per unit Golgi area (n = 8 cells).

(C and D) Maximum projections of 3D confocal acquisitions in the Golgi area before (top) and after (bottom) the application of a mechanical constraint. The number of LifeAct-mCherry patches colocalizing with the Golgi marker was scored per unit Golgi area (n = 12 cells).

(E and F) A force was applied on the Golgi complex of GFP-Rab6-expressing cells for 1 min (bottom). In control cells, no constraint was applied (top). Cells were then fixed and labeled for cortactin. The number of cortactin patches colocalizing with GFP-Rab6 was scored per unit Golgi area (n = 10 cells).

In (A), (C), and (E), the signal-to-noise ratio in the raw images (left) was improved using the ndSafir denoising algorithm [46] (middle and right). Beads are shown in white, actin or cortactin in red, and the Golgi marker in green. The blue arrow indicates the direction of the force. Arrowheads point to actin or cortactin patches. Scale bars represent 5 μm. Error bars represent mean ± SEM. See also Movie S4.

case, which we refer to as "bead ejection," the bead followed the displacement of the stage or was actively pushed farther away from the trap center. To characterize the rigidity of the microenvironment of the bead, we defined and measured three parameters: the bead step amplitude, the softness index, and the frequency of bead ejection. The bead step amplitude corresponds to the displacement of the bead after a 0.5 μm step displacement of the piezo-stage. The softness index is defined by $s = (d_{piezo} - d_{bead}) / d_{piezo}$, where d_{bead} and d_{piezo} are the displacements of the bead within the trap and of the piezo-stage, respectively. If the viscous drag is larger than the trapping force and the bead is no longer held in the trap, $d_{piezo} = d_{bead}$ and $s = 0$. If the bead is pushed out of the trap, d_{bead} can be greater than d_{piezo} and s can take negative values. The frequency of bead ejection is the number of cases where the bead falls off the optical trap after a 0.5 μm piezo-stage displacement step during an experiment lasting 1 min.

Colocalization of GFP-Rab6 Signals before and after Application of a Mechanical Constraint

Two dual-color confocal stacks were acquired to image Rab6-positive Golgi membranes and the optically trapped bead before and after application of a 100–200 pN force by manual displacement of the stage for 1 min. Control experiments were performed similarly except that the stage position remained fixed during 1 min between the first and second confocal stack acquisitions. Colocalization was quantified with ImageJ and the JACoP plug-in [45].

Quantification of the Transport of Rab6-Positive Intermediates

Rab6-positive transport intermediates were imaged at 1 frame/s using the galvanometric mode averaging to increase the signal to noise ratio of the confocal images. Time-lapse movies were taken during 1 min. Movements of Rab6-positive intermediates from or toward the Golgi complex were discriminated by superimposing two kymographs along two lines drawn parallel to the Golgi complex but separated by a few pixels (Figure S3 and Supplemental Experimental Procedures).

Statistical Analysis

Results are representative of at least three independent experiments. Data are expressed as means ± standard error mean. Statistical relevance was evaluated with Student's t tests and the p value is indicated (n.s., nonsignificant; *p < 0.1, **p < 0.05, ***p < 0.001).

Supplemental Information

Supplemental Information includes five figures, Supplemental Experimental Procedures, and five movies and can be found with this article online at http://dx.doi.org/10.1016/j.cub.2014.06.048.

Acknowledgments

We thank Patricia Bassereau, Benoît Sorre, Aurélien Roux, Gil Toombes, and Xavier Mezanges for assistance in the design of the experimental set-up. We thank Rob Phillips, Pierre Sens, Bruno Antonny, Cathy Jackson, Samuel Bouvet, Jean Salamero, Catherine Dargemont, Stéphanie Miserey-Lenkei, and Giovanni Capello for stimulating discussions. This work was in part performed within the Nikon Imaging Center @ Institut Curie. Assistance from the BioImaging Cell and Tissue Core Facility of the Institut Curie (*PICT-IBiSA*) is acknowledged. D.G. is funded by a grant from the French Ministry of Research. Other funding is from Institut Curie, CNRS (Program "Prise de risque à l'interface Physique-Biologie"), ANR (grant number ANR09-JCJC-0020-01), and INSERM Plan Cancer 2009-2013 INSERM - CEA Tecsan (grant number PC201125).

Received: April 2, 2013
Revised: May 6, 2014
Accepted: June 18, 2014
Published: July 17, 2014

References

1. Lowe, M. (2011). Structural organization of the Golgi apparatus. Curr. Opin. Cell Biol. *23*, 85–93.
2. Egea, G., Lázaro-Diéguez, F., and Vilella, M. (2006). Actin dynamics at the Golgi complex in mammalian cells. Curr. Opin. Cell Biol. *18*, 168–178.
3. Chen, J.-L., Lacomis, L., Erdjument-Bromage, H., Tempst, P., and Stamnes, M. (2004). Cytosol-derived proteins are sufficient for Arp2/3 recruitment and ARF/coatomer-dependent actin polymerization on Golgi membranes. FEBS Lett. *566*, 281–286.
4. Dubois, T., Paléotti, O., Mironov, A.A., Fraisier, V., Stradal, T.E.B., De Matteis, M.A., Franco, M., and Chavrier, P. (2005). Golgi-localized GAP for Cdc42 functions downstream of ARF1 to control Arp2/3 complex and F-actin dynamics. Nat. Cell Biol. *7*, 353–364.
5. Carreno, S., Engqvist-Goldstein, A.E., Zhang, C.X., McDonald, K.L., and Drubin, D.G. (2004). Actin dynamics coupled to clathrin-coated vesicle formation at the trans-Golgi network. J. Cell Biol. *165*, 781–788.
6. di Campli, A., Valderrama, F., Babià, T., De Matteis, M.A., Luini, A., and Egea, G. (1999). Morphological changes in the Golgi complex correlate with actin cytoskeleton rearrangements. Cell Motil. Cytoskeleton *43*, 334–348.
7. Kondylis, V., van Nispen tot Pannerden, H.E., Herpers, B., Friggi-Grelin, F., and Rabouille, C. (2007). The golgi comprises a paired stack that is separated at G2 by modulation of the actin cytoskeleton through Abi and Scar/WAVE. Dev. Cell *12*, 901–915.
8. Brownhill, K., Wood, L., and Allan, V. (2009). Molecular motors and the Golgi complex: staying put and moving through. Semin. Cell Dev. Biol. *20*, 784–792.
9. Miserey-Lenkei, S., Chalancon, G., Bardin, S., Formstecher, E., Goud, B., and Echard, A. (2010). Rab and actomyosin-dependent fission of transport vesicles at the Golgi complex. Nat. Cell Biol. *12*, 645–654.
10. Dippold, H.C., Ng, M.M., Farber-Katz, S.E., Lee, S.K., Kerr, M.L., Peterman, M.C., Sim, R., Wiharto, P.A., Galbraith, K.A., Madhavarapu, S., et al. (2009). GOLPH3 bridges phosphatidylinositol-4- phosphate and actomyosin to stretch and shape the Golgi to promote budding. Cell *139*, 337–351.
11. Anitei, M., and Hoflack, B. (2012). Bridging membrane and cytoskeleton dynamics in the secretory and endocytic pathways. Nat. Cell Biol. *14*, 11–19.
12. Zilberman, Y., Alieva, N.O., Miserey-Lenkei, S., Lichtenstein, A., Kam, Z., Sabanay, H., and Bershadsky, A. (2011). Involvement of the Rho-mDia1 pathway in the regulation of Golgi complex architecture and dynamics. Mol. Biol. Cell *22*, 2900–2911.
13. Manneville, J.-B., Casella, J.-F., Ambroggio, E., Gounon, P., Bertherat, J., Bassereau, P., Cartaud, J., Antonny, B., and Goud, B. (2008). COPI coat assembly occurs on liquid-disordered domains and the associated membrane deformations are limited by membrane tension. Proc. Natl. Acad. Sci. USA *105*, 16946–16951.
14. Pinot, M., Goud, B., and Manneville, J.-B. (2010). Physical aspects of COPI vesicle formation. Mol. Membr. Biol. *27*, 428–442.
15. Gauthier, N.C., Masters, T.A., and Sheetz, M.P. (2012). Mechanical feedback between membrane tension and dynamics. Trends Cell Biol. *22*, 527–535.
16. Boulant, S., Kural, C., Zeeh, J.-C., Ubelmann, F., and Kirchhausen, T. (2011). Actin dynamics counteract membrane tension during clathrin-mediated endocytosis. Nat. Cell Biol. *13*, 1124–1131.
17. Römer, W., Pontani, L.L., Sorre, B., Rentero, C., Berland, L., Chambon, V., Lamaze, C., Bassereau, P., Sykes, C., Gaus, K., and Johannes, L. (2010). Actin dynamics drive membrane reorganization and scission in clathrin-independent endocytosis. Cell *140*, 540–553.
18. Matas, O.B., Martínez-Menárguez, J.A., and Egea, G. (2004). Association of Cdc42/N-WASP/Arp2/3 signaling pathway with Golgi membranes. Traffic *5*, 838–846.
19. Ashkin, A., Schütze, K., Dziedzic, J.M., Euteneuer, U., and Schliwa, M. (1990). Force generation of organelle transport measured in vivo by an infrared laser trap. Nature *348*, 346–348.
20. Hosokawa, C., Kudoh, S.N., Kiyohara, A., and Taguchi, T. (2011). Optical trapping of synaptic vesicles in neurons. Appl. Phys. Lett. *98*, 163705.
21. van der Honing, H.S., de Ruijter, N.C., Emons, A.M., and Ketelaar, T. (2010). Actin and myosin regulate cytoplasm stiffness in plant cells: a study using optical tweezers. New Phytol. *185*, 90–102.
22. Welte, M.A., Gross, S.P., Postner, M., Block, S.M., and Wieschaus, E.F. (1998). Developmental regulation of vesicle transport in *Drosophila* embryos: forces and kinetics. Cell *92*, 547–557.
23. Robert, D., Nguyen, T.-H., Gallet, F., and Wilhelm, C. (2010). In vivo determination of fluctuating forces during endosome trafficking using a combination of active and passive microrheology. PLoS ONE *5*, e10046.
24. Hendricks, A.G., Holzbaur, E.L.F., and Goldman, Y.E. (2012). Force measurements on cargoes in living cells reveal collective dynamics of microtubule motors. Proc. Natl. Acad. Sci. USA *109*, 18447–18452.

25. Shekhar, S., Cambi, A., Figdor, C.G., Subramaniam, V., and Kanger, J.S. (2012). A method for spatially resolved local intracellular mechanochemical sensing and organelle manipulation. Biophys. J. *103*, 395–404.
26. Rai, A.K., Rai, A., Ramaiya, A.J., Jha, R., and Mallik, R. (2013). Molecular adaptations allow dynein to generate large collective forces inside cells. Cell *152*, 172–182.
27. Blehm, B.H., Schroer, T.A., Trybus, K.M., Chemla, Y.R., and Selvin, P.R. (2013). In vivo optical trapping indicates kinesin's stall force is reduced by dynein during intracellular transport. Proc. Natl. Acad. Sci. USA *110*, 3381–3386.
28. Veigel, C., and Schmidt, C.F. (2011). Moving into the cell: single-molecule studies of molecular motors in complex environments. Nat. Rev. Mol. Cell Biol. *12*, 163–176.
29. Mikhailenko, S.V., Oguchi, Y., and Ishiwata, S. (2010). Insights into the mechanisms of myosin and kinesin molecular motors from the single-molecule unbinding force measurements. J. R. Soc. Interface *7* (*Suppl 3*), S295–S306.
30. Deguchi, S., Ohashi, T., and Sato, M. (2006). Tensile properties of single stress fibers isolated from cultured vascular smooth muscle cells. J. Biomech. *39*, 2603–2610.
31. Hotulainen, P., and Lappalainen, P. (2006). Stress fibers are generated by two distinct actin assembly mechanisms in motile cells. J. Cell Biol. *173*, 383–394.
32. Desai, A., and Mitchison, T.J. (1997). Microtubule polymerization dynamics. Annu. Rev. Cell Dev. Biol. *13*, 83–117.
33. Kalwarczyk, T., Ziebacz, N., Bielejewska, A., Zaboklicka, E., Koynov, K., Szymański, J., Wilk, A., Patkowski, A., Gapiński, J., Butt, H.-J., and Hołyst, R. (2011). Comparative analysis of viscosity of complex liquids and cytoplasm of mammalian cells at the nanoscale. Nano Lett. *11*, 2157–2163.
34. Parker, W.C., Chakraborty, N., Vrikkis, R., Elliott, G., Smith, S., and Moyer, P.J. (2010). High-resolution intracellular viscosity measurement using time-dependent fluorescence anisotropy. Opt. Express *18*, 16607–16617.
35. Van Citters, K.M., Hoffman, B.D., Massiera, G., and Crocker, J.C. (2006). The role of F-actin and myosin in epithelial cell rheology. Biophys. J. *91*, 3946–3956.
36. Hvidt, S., and Janmey, P.A. (1990). Elasticity and flow properties of actin gels. Makromolekulare Chemie. Macromol. Symp. *39*, 209–213.
37. Zaner, K.S., and Valberg, P.A. (1989). Viscoelasticity of F-actin measured with magnetic microparticles. J. Cell Biol. *109*, 2233–2243.
38. Bausch, A.R., Ziemann, F., Boulbitch, A.A., Jacobson, K., and Sackmann, E. (1998). Local measurements of viscoelastic parameters of adherent cell surfaces by magnetic bead microrheometry. Biophys. J. *75*, 2038–2049.
39. Mackintosh, F.C., and Schmidt, C.F. (2010). Active cellular materials. Curr. Opin. Cell Biol. *22*, 29–35.
40. Joanny, J.-F., and Prost, J. (2009). Active gels as a description of the actin-myosin cytoskeleton. HFSP J *3*, 94–104.
41. Kovács, M., Thirumurugan, K., Knight, P.J., and Sellers, J.R. (2007). Load-dependent mechanism of nonmuscle myosin 2. Proc. Natl. Acad. Sci. USA *104*, 9994–9999.
42. Römer, W., Berland, L., Chambon, V., Gaus, K., Windschiegl, B., Tenza, D., Aly, M.R., Fraisier, V., Florent, J.C., Perrais, D., et al. (2007). Shiga toxin induces tubular membrane invaginations for its uptake into cells. Nature *450*, 670–675.
43. Schauer, K., Duong, T., Bleakley, K., Bardin, S., Bornens, M., and Goud, B. (2010). Probabilistic density maps to study global endomembrane organization. Nat. Methods *7*, 560–566.
44. Pinot, M., Chesnel, F., Kubiak, J.Z., Arnal, I., Nedelec, F.J., and Gueroui, Z. (2009). Effects of confinement on the self-organization of microtubules and motors. Curr. Biol. *19*, 954–960.
45. Bolte, S., and Cordelières, F.P. (2006). A guided tour into subcellular colocalization analysis in light microscopy. J. Microsc. *224*, 213–232.
46. Boulanger, J., Kervrann, C., Bouthemy, P., Elbau, P., Sibarita, J.-B., and Salamero, J. (2010). Patch-based nonlocal functional for denoising fluorescence microscopy image sequences. IEEE Trans. Med. Imaging *29*, 442–454.